This pre-print is currently under review at LIMNOLOGY & OCEANOGRAPHY - LETTERS and has been peer reviewed and approved for publication consistent with U.S. Geological Survey Fundamental Science Practices (pubs.usgs.gov/circ/1367/).

The extended Global Lake area, Climate, and Population (GLCP) dataset: Extending the GLCP to include ice, snow, and radiation-related climate variables

Michael F Meyer[1,2], Salvatore GP Virdis[3], Xiao Yang[4], Matthew R Brousil[5], Ryan P McClure[6], Sapna Sharma[7], R Iestyn Woolway[8], Alli N Cramer[9], Jianning Ren[10], Stephen L Katz[11], Stephanie E Hampton[6], Haoran Shi[8]

[1.] U.S. Geological Survey, Water Resources Mission Area, Observing Systems Division - Hydrologic Remote Sensing Branch, Madison, WI, USA
[2.] Center for Limnology, University of Wisconsin - Madison, Madison, WI, USA
[3.] Department of Information & Communication Technologies, School of Engineering and Technology, Asian Institute of Technology, Pathum Thani, Thailand
[4.] Department of Earth Sciences, Southern Methodist University, Dallas, TX, USA
[5.] Ecosystem Science and Sustainability, Colorado State University, Fort Collins, CO, USA
[6.] Biosphere Sciences and Engineering, Carnegie Institution for Science, Pasadena, CA, USA
[7.] Biology Department, York University, Toronto, ON, Canada
[8.] School of Ocean Sciences, Bangor University, Menai Bridge, UK
[9.] School of Mathematical and Natural Sciences, Arizona State University, Phoenix, AZ, USA
[10.] Department of Civil and Environmental Engineering, National University of Singapore, Singapore
[11.] Sharper Informatics Solutions, Seattle, WA, USA

Author Contribution Statement: MFM conceived the idea for, designed, and provided leadership for the manuscript. MFM, SPGV, XY, MRB, RPM, and ANC contributed to data harmonization. MFM, SGPV, RIW, SLK, and HS contributed to figure development. MFM, SGPV, XY, MRB, RPM, SS, RIW, ANC, JR, SLK, and HS contributed to quality control checks during the creation of the dataset. MFM, SGPV, XY, SS, RIW, and SH wrote original text for the manuscript, which was revised by MFM, SGPV, SS, RMP, JR, and ANC. All authors read and approved the final manuscript.

Corresponding author Email: mfmeyer@usgs.gov

Grant sponsor information: Funding was provided in part by a NSF Graduate Research Fellowship (NSF-DGE-1347973), a U.S. Geological Survey Water Resources Mission Area Mendenhall Fellowship, and from the U.S. Geological Survey Saline Lake Ecosystems Integrated Water Availability Assessment Program to MFM.

Key Words (10 max): limnology, global water cycle, hydrology, remote sensing, climate reanalysis

URL of the Dataset and Metadata with permanent identifier:
https://doi.org/10.6073/pasta/e0bf4571ca6cbfb81c3ed7caefc85fc6

Code URL with permanent identifier:
https://doi.org/10.6073/pasta/e0bf4571ca6cbfb81c3ed7caefc85fc6

Measurement(s): Seasonal and permanent lake surface area, fractional lake ice cover, basin snow area, air temperature, precipitation, specific humidity, shortwave radiation, longwave radiation, fractional cloud cover

Technology Type(s): Remote Sensing, Climate Reanalysis

Temporal range: January 1995 through December 2020

Frequency or sampling interval: Monthly

Spatial scale: Globally within 78°N and 78°S

Abstract (147 of 150 words)

A changing climate and increasing human population necessitate understanding global freshwater availability. To enable assessment of lake water variability from local-to-global and monthly-to-decadal scales, we extended the Global Lake area, Climate, and Population (GLCP) dataset, which contains monthly lake surface area for 1.42 million lakes with paired basin-level climate and population data from 1995 through 2020. In comparison to the previous version of the GLCP, the extended version is monthly and includes information on lake ice cover as well as basin-level snow area, humidity, longwave and shortwave radiation, and cloud cover. The extended GLCP emphasizes FAIR data principles by expanding its scripting repository and maintaining unique HydroLAKES identifiers, which enables the GLCP to be joined with other HydroLAKES-derived products. Compared to the original version, the extended GLCP contains a richer suite of variables that enable disparate analyses of lake water trends at broad spatial and temporal scales.

Scientific Significance Statement

We present the extended Global Lake area, Climate, and Population (GLCP) dataset, a tabular, analysis-ready dataset of monthly lake surface area and ice cover with paired basin-wide temperature, precipitation, humidity, cloud cover, shortwave radiation, longwave radiation, snow cover, and human population residing in the basin over 25 years. Although similar in structure to its previous version, the extended GLCP expands the temporal resolution from annual to monthly time-steps, the time scale from 1995-2015 to 1995-2020, and the variable content, thereby empowering investigations of lake responses to ice and snow loss as well as solar radiation change. By harmonizing these variables to a lake and its associated basin, the extended GLCP is the most expansive, publicly available dataset that merges lake information for over 1.42 million lakes globally across two satellite missions, climate reanalysis, and human demography datasets. With a reproducible, scripted workflow, the dataset is also customizable and enables users to adapt scripts to incorporate particular variables of interest.

Background and Motivation

Freshwater is an essential resource, unevenly distributed across the globe, and facing increasing pressures from a changing climate and anthropogenic activities (Vörösmarty et al. 2000, 2018). The most readily accessible freshwater for human use is in surface waters, which represent less than 1% of the planet's water supply (Jones and Smol 2023). The majority of surface freshwater is found in lakes, which are predominantly distributed in northern regions of the planet (Verpoorter et al. 2014; Messager et al. 2016). Increasing temperatures and changing precipitation regimes are among the most well studied climatic drivers of hydrologic change (Woolway et al. 2020), yet, understanding lake dynamics requires not only traditional climate variables, like temperature and precipitation, but also radiation-related variables. Solar radiation, for instance, plays a crucial role in lake water temperature, evaporation rates, and ultimately, lake water availability (O'Reilly et al. 2015). Changes in solar radiation thus can substantially affect lake ecosystems and their surrounding environments. Considering the complexity of environmental drivers, there is a need for deeper understanding of how a shifting climate and

changing human demand contributes to the ongoing and projected alterations in the global water cycle (Vörösmarty et al. 2018).

Global and regional trends in lake water availability have been documented (Yao et al. 2023; Zhou et al. 2024), however, predicting future water availability requires a more comprehensive understanding of the mechanisms driving these trends. Analyses, particularly in arid regions, have revealed significant declines in water storage between 1992 and 2020 (Yao et al., 2023). These declines are more pronounced in arid areas, whereas northern regions exhibit variability, with some lakes growing and others shrinking depending on basin-specific hydrologic processes (Yao et al. 2023). Melting mountain glaciers can lead to expanding lake surfaces, as observed in regions like the Himalayas (Zhou et al. 2024). Conversely, as seen in the high Arctic, melting permafrost can decrease lake surface area due to increased seepage (Webb et al. 2022). These contrasting examples highlight the complexity of lake responses to environmental drivers.

Given the rapid pace of climatic change worldwide and a growing human population, analyzing water availability patterns and their relationships with potential drivers can inform projections of future change, motivating synthesis of existing data. The availability of remote sensing, climate reanalysis, and *in situ* data to address global water cycle changes has never been greater, enabling analyses at various spatial and temporal scales. For example, the Moderate Resolution Imaging Spectroradiometer (MODIS) facilitates lake ice and snow monitoring (Hall et al. 2002), whereas Landsat and Sentinel-2 facilitate global surface water extent products (Pekel et al. 2016; Jones 2019). The Modern-Era Retrospective analysis for Research and Applications, version 2 (MERRA-2) and ERA5 datasets have revolutionized the study of temperature and precipitation changes (Gelaro et al. 2017; Hersbach et al. 2020). Although each product offers immense value, working with this expanding data pool becomes increasingly complex. Researchers must make informed choices about harmonizing these diverse data sources, ensuring accessibility to a user community with varied skill sets and available infrastructure, and also accurately reflecting real-world ecosystems.

To accelerate future research and begin to bridge existing data gaps, we present the extended Global Lake area, Climate, and Population (GLCP) dataset (Labou et al. 2019; Meyer et al. 2020, 2024a), a compendium of lake surface area, climate reanalysis, snow and ice products, as well as human population data. The extended GLCP dataset is a resource to support researchers investigating lake dynamics and their connection to climate change, human population growth, and other environmental factors. This comprehensive dataset allows for in-depth analyses of historical trends and future projections, thereby fostering a more nuanced understanding of lakes worldwide. The tabular, analysis-ready format of the GLCP facilitates accessibility for researchers with varying technical expertise, promoting broader use and potentially leading to novel scientific discoveries. Furthermore, the inclusion of human population data allows for the exploration of the intricate relationship between water resource availability and population changes, potentially informing strategies for sustainable water management practices.

Data Description

The extended GLCP is available in a tabular format from the Environmental Data Initiative (Meyer et al. 2024a). We distributed the extended GLCP among 14 .csv files. With the exception of North America, each continent is an individual file. North America is split between lakes in Canada and lakes in other North American countries. Lakes in Canada are divided into 8 .csv files, because one file for all lakes in Canada would likely be too large for many end users working with the data locally. Figure 1 highlights the distribution of lakes included in the GLCP.

Each file of the GLCP has a tabular structure as described below:

HYBAS_ID: Unique basin identifier from HydroBASINS (Lehner and Grill 2013).

year: Year of observations.

month: Numerical month of observations

Hylak_id: Unique lake identifier from HydroLAKES (Messager et al. 2016).

seasonal_km2: Annual seasonal lake surface area. Seasonal surface area is defined as the sum of pixels identified as water for at least one month within one calendar year but not for all observable months in a calendar year.

permanent_km2: Annual permanent lake surface area. Permanent surface area is defined as the sum of pixels identified as water for all observable months in a calendar year.

country: Country in which a lake is located, as defined by HydroLAKES (Messager et al. 2016).

continent: Continent in which a lake is located, as defined by HydroLAKES (Messager et al. 2016).

Center_Lat: Lake centroid latitude.

Center_Lon: Lake centroid longitude.

mean_spec_humidity: Mean, monthly basin-level specific humidity, in grams of water per grams of air.

mean_precip_mm: Mean, monthly basin-level precipitation, in millimeters.

mean_temp_k: Mean, monthly basin-level temperature, in Kelvin.

mean_totcloud_pct: Mean, monthly basin-level cloud cover, expressed as a proportion of the lake's basin.

mean_sw_wm2: Mean, monthly basin-level shortwave radiation, in Watts per square meter.

mean_lw_wm2: Mean, monthly basin-level longwave radiation, in Watts per square meter.

monthly_water_area_km2: Surface area measurement for a given lake in a specific month-year combination, in square kilometers.

pop_sum: Number of people living within a basin. Because fractional areas are considered when aggregating pixels within a basin, values for the number of people living within a basin can have floating decimals.

ice_cover_min: Minimum percentage of lake ice cover within a month.

ice_cover_max: Maximum percentage of lake ice cover within a month.

ice_cover_mean: Mean percentage of lake ice cover within a month.

ice_cover_median: Median percentage of lake ice cover within a month.

ice_cover_binary_min: Similar to **ice_cover_min**, except that pixels with less than 15% ice cover are removed before calculating ice cover percentage.

ice_cover_binary_max: Similar to **ice_cover_max**, except that pixels with less than 15% ice cover are removed before calculating ice cover percentage.

ice_cover_binary_mean: Similar to **ice_cover_mean**, except that pixels with less than 15% ice cover are removed before calculating ice cover percentage.

ice_cover_binary_median: Similar to **ice_cover_median**, except that pixels with less than 15% ice cover are removed before calculating ice cover percentage.

ice_cover_count: Number of images used within a month for estimating lake ice cover statistics.

snow_min: Minimum percentage of basin snow area cover.

snow_mean: Mean percentage of basin snow area cover.

snow_max: Maximum percentage of basin snow area cover.

snow_valid_count: Number of valid snow observations in a month.

snow_invalid_count: Number of invalid snow observations in a month.

snow_area: Area of a basin covered with snow, based on the mean fractional snow area.

Methods

Input Data Sources

HydroLAKES

We used the HydroLAKES database version 1.0 (Messager et al. 2016) to identify lake location. HydroLAKES incorporates multiple lake datasets (e.g., Shuttle Radar Topology Mission, Water Body Data, Global Lakes and Wetlands Database) to provide shapefile outlines of 1,427,688 lakes of at least 10 hectares in surface area. The majority of HydroLAKES' lakes are defined as uncontrolled lakes (99.5%), with the remainder identified as reservoirs (0.47%) and controlled lakes (0.03%). The HydroLAKES v1.0 identifier ("Hylak_id") is retained in the GLCP to facilitate interoperability. Like the previous version of the GLCP, we have included the columns "Center_Lat" and "Center_Lon" to indicate the latitude and longitude of the lakes' centroids. Hereafter, HydroLAKES lake polygons are referred to as "lakes".

HydroBASINS

Because lakes are products of the landscapes in which they reside, we calculated climate and human population using the HydroBASINS dataset (Lehner and Grill 2013), a basin-level analog to the HydroLAKES dataset. The HydroBASINS version 1.c format 1 database includes 3,786,218 unique basins and is derived from the HydroSHEDS database (Lehner and Grill 2013), which uses 15 arc-second resolution data to identify catchments globally. In HydroBASINS, basins are identified using the Pfafstetter coding system (Verdin and Verdin 1999), with Level 1 as the highest level (i.e., continent level) and Level 12 as the smallest available sub-basin. We retain the original HydroBASINS identifier ("HYBAS_ID") for each basin in the GLCP, for ease of integration with existing HydroBASINS attributes and derived products.

Joint Research Centre Global Surface Water Extent Dataset

To estimate lake surface area over time, we used the Joint Research Centre (JRC) Global Surface Water Extent Dataset described in Pekel et al. (2016), which uses Landsat imagery (30-meter resolution) from March 1984 through present day to identify surface water globally. For the creation of the extended GLCP, we used JRC products from January 1995 through December 2020. Hereafter, we use the abbreviation "JRC" to refer to this dataset.

The JRC data are publicly available through Google Earth Engine (Gorelick et al. 2017) as well as the European Commission data portal (global-surface-water.appspot.com) as annual and monthly aggregated raster images. For annual data, images contain information about pixels coded as "not water", "seasonal water" (defined as liquid water that is present for at least one month but not all observed months in a calendar year), and "permanent water" (defined as liquid water that is present for all observed months in a calendar year). For monthly data, the JRC provides monthly rasters within each year with data on whether a pixel was classified as "water" or "not water". In an ideal case, these classifications come from approximately fortnightly observations, although classifications could be made of single or interpolated values, depending

on the image quality and time a given classification estimate was made. For example, particularly cloudy regions may experience greater missing data, and therefore, fewer surface water observations. Similarly, entire regions may experience greater missing data due to limited satellite coverage. In particular, the Kolyma region in northeast Siberia has notable data sparsity 1995-1999 due to only one Landsat satellite being in orbit. For more detailed information on the complete workflow used to create the JRC, Pekel et al. (2016) provides a methodology of how water pixels are assigned.

Even with its robust classification system, the JRC is limited to classifying liquid surface water, where ice and snow in images could be coded as non-water. This system, therefore, does not classify permanently frozen lakes as water. Seasonally frozen lakes, however, could be coded as entirely seasonal water if valid observations for a waterbody exist for all 12 months of an observing year. In instances where valid observations may only be present for less than 12 months, the number of months required to classify a water pixel as seasonal or permanent depends on the number of observable months within that calendar year. For example, if a water pixel had 8 months of observable water, then a pixel classified as water for all 8 months would be considered “permanent water”, whereas a pixel classified as water for at least 1 month but not all 8 months would be classified as “seasonal water”.

Modern-Era Retrospective analysis for Research and Applications V2

We used the Modern-Era Retrospective analysis for Research and Applications, Version 2 (MERRA-2) as the source for climate data from 01 January 1995 through 31 December 2020 (Gelaro et al. 2017). All climate datasets were hourly aggregates with original spatial resolution of 0.5 × 0.625 decimal degrees. From these broader datasets, we extracted the variables bias corrected, total precipitation over land (PRECTOTCORRLAND; kg m^{-2} s^{-1} or volumetrically, mm s^{-1}), 2-meter air temperature (T2M; Kelvin), 2-meter humidity (QV2M; kg/kg), total cloud area fraction (CLDTOT), net downward longwave radiation flux (LWGNT; Wm^{-2}), and net downward shortwave radiation flux (SWGNT; Wm^{-2}). These MERRA-2 data were exported from NASA Goddard Earth Sciences Data and Information Services Center (disc.gsfc.nasa.gov) in a netCDF format.

Although many climate reanalysis products exist (e.g., ERA5), the choice to use MERRA-2 stemmed from the previous version of the GLCP incorporating MERRA-2 data, which was the most spatially and temporally extensive climate reanalysis dataset at the time. To ensure that the extended GLCP remained compatible with the previous version, we elected to only aggregate climate variables with MERRA-2 products. Users interested in aggregating an alternative climate reanalysis dataset in a manner similar to the GLCP can adapt the scripts provided in "gee_scripts.zip” as well as “R_scripts.zip”, although the extent to which alternative reanalysis datasets reflect values and trends from MERRA-2 would depend on the assumptions and methods developed for those respective datasets.

Gridded Population of the World

We used the Global Rural-Urban Mapping Project (GRUMP) dataset for 1995 and Gridded Population of the World (GPW) version 4.11 adjusted population count data for 2000, 2005,

2010, 2015, and 2020 population estimates (Doxsey-Whitfield et al. 2015). Building off GPWv3, the GRUMP dataset corrects human population estimates in rural areas, whereas the original GPWv3 dataset tends to be less robust at predicting rural populations. Resolution for GRUMP is 2.5 arc-minutes, whereas resolution for GPW version 4.11 is 30 arc-seconds and is currently hosted on Google Earth Engine. Detailed methodology for the development of these datasets is available in Doxsey-Whitfield et al. (2015).

Moderate Resolution Imaging Spectroradiometer (MODIS) Snow and Ice products

For both snow and ice cover estimates, we used the MODIS onboard the Terra satellite from 2001 through 2020. However, the exact MODIS product used for snow and ice cover estimates differed because basins' large areas (>1,000 km) often produced computational memory limitations. For lake ice area estimates, we used the MOD10A1 (version 6) Snow Cover Daily Global 500-m product (product guide can be accessed at https://nsidc.org/sites/default/files/mod10a1-v006-userguide_3.pdf). For snow area estimates, we used the MODIS/Terra Snow Cover Monthly L3 Global 0.05 Decimal Degree resolution which offers a resolution of 5 km. Snow and ice cover were classified using the normalized difference snow index (NDSI; Hall and Riggs 2011), which incorporates the MODIS band 4 and band 6 with additional data screening procedures to flag the data quality. For example, overall spectral reflectance and thermal band data are used to combat commission errors, and the use of a forested region-specific threshold for NDSI to account for the influence from vegetation canopy. In the resulting data, each pixel in the "NDSI_Snow_Cover" band of the daily image has values from 0–100 representing the snow cover for that pixel, with values outside of this range used as flags for poor data quality or missing data (e.g., cloud obstruction).

Harmonization Procedure

The extended GLCP dataset is constructed in a six-step pipeline depicted in Figure 2. Each step of creating the extended GLCP is detailed below.

Step 1: Calculate lake-level annual seasonal, annual permanent, and monthly water area

Lake area estimates are derived by extracting seasonal and permanent water area from the JRC (Pekel et al. 2016) located within 90 m of predefined lake shapefiles (Messager et al. 2016). Meyer et al. (2020) provides analyses showing that a 90-m buffer captures the majority of lake area fluctuation beyond the static lake shapefiles, while also minimizing the chance of including external water bodies into a target lake's surface area. Due to increased temporal resolution of the JRC, we also estimated monthly areas for all lakes. Google Earth Engine scripts used for aggregation are available in Meyer et al. (2024a).

Step 2: Calculate lake-level fractional ice area cover

We estimated monthly lake ice coverage using MODIS daily snow cover (NDSI_Snow_Cover) product and the HydroLAKES database. Each daily snow cover image quantifies snow covered areal percentage into values from 0% to 100%, with values masked out for areas of missing data,

low light condition, and cloud cover. For each day, snow cover images were used to estimate ice areal percent coverage for each lake using the following steps:

1. A daily snow cover image was first converted to a binary image of ice (1) and non-ice (0) using 15% as the minimum threshold. Pixels with values ≥ 15% were assumed to be ice cover. The resulting binary ice image was then appended to the original snow cover fraction image as an additional band.

2. Lake ice fraction and missing data fraction were estimated by calculating fractional cover of ice pixels and missing data pixels over the entire lake polygon region.

3. If the missing data fraction for a given day exceeded 20%, the observation was discarded from further aggregation.

Once we obtained the daily lake ice fractions and removed the observations that contained substantial missing data (>20%) over the lake surface, we calculated minimum, maximum, mean, median, and number of valid observations for a given lake-year-month combination.

Although the above worked well for smaller lakes, we encountered memory limitations in Google Earth Engine for lakes greater than 64 km^2. We resolved these memory limitation issues by reducing the resolution of the image for the lakes with surface area greater than 64 km^2 before calculating the daily lake ice fractions. The resolution used in the calculation for the large lakes was implemented so that it scaled with the size of the lake surface.

Step 3: Calculate basin-level climate estimates

Monthly climate values for each basin in the extended GLCP were calculated following the procedure outlined in Meyer et al. (2020). Each daily climate raster, except for precipitation, was averaged within a given year-month combination, and then exported as a monthly raster. For precipitation, volumetric precipitation within a pixel was calculated by summing precipitation values within a pixel across a month. Monthly rasters were resampled at 1/10th cell size using a bilinear interpolation. Resampled rasters were then exported to Google Earth Engine, where basin-wide averages were calculated for each climate variable and raster. Scripts for aggregation are available in Meyer et al. (2024a).

Step 4: Calculate basin-level human population estimates

Following methods described in Meyer et al. (2020), human population was summed within each lake's basin for each year of the GPW. Population rasters were aggregated to basin-level summations in Google Earth Engine. Notably, this process created fractional populations residing within a basin, due to Google Earth Engine reducers weighting partial pixels within a basin. These fractional persons are expected in the dataset, and floating decimals are retained. Scripts for aggregation are available in Meyer et al. (2024a).

Step 5: Calculate multi-scale basin-level fractional snow area cover

Using the MODIS Global Level-3 Snow dataset, we calculated summary statistics of snow area cover within a given basin-year-month combination. Basins smaller than 25 km^2 were removed from the analysis, due to the fact that they may have insufficient pixels to make an accurate assessment. Final summary statistics for each basin included the maximum, minimum, and mean snow fractional area cover, the total snow area covered by the mean fractional cover, as well as the number of valid and invalid pixels occurring within a given basin in a particular month. Python scripts used to aggregate snow basin data are available in Meyer et al. (2024a).

Step 6: Merge lake- and basin-level data products

All resulting derived products were merged into a single .csv, with a matching procedure described in Meyer et al. (2020). Due to large file sizes, each continent is contained within its own .csv, with the exception of North America. Lakes in Canada were split into 8 separate .csv files, and all remaining lakes in North America are contained in a separate .csv file.

Outside of Google Earth Engine, all data aggregation and harmonization, with the exception of snow cover, occurred within the R Statistical Environment (R Core Team 2022), using the tidyverse (Wickham et al. 2019), data.table (Dowle and Srinivasan 2021), lubridate (Grolemund and Wickham 2011), stringr (Wickham 2019), and hexbin (Carr et al. 2021) packages. Snow aggregation was performed in Python v 2.5.1 using the pandas (McKinney and others 2010), geopandas (Jordahl 2014), numpy (Harris et al. 2020), and rasterio (Gillies and others 2013) libraries. Platform-specific scripts can be accessed in the corresponding compressed entity on the Environmental Data Initiative (i.e., “gee_script.zip”, “R_scripts.zip”, and “python_scripts.zip”).

Technical Validation

For the extended GLCP, we repeated all validation procedures detailed in Meyer et al. (2020) to ensure that the updated version is consistent with the previous version. Here, we expand upon additional validation procedures that we implemented in Meyer et al. (2020) to ensure data integrity did not degrade during data harmonization.

Zero-area and NA-area lakes

For annual permanent and seasonal lake area estimates, the extended GLCP contains a large number of lakes with zero-area observations for at least one year during the period of 1995 through 2020 (n = 430,961; 30.2%), but a small fraction has zero areas for the entire period from 1995 through 2020 (n = 9,563; 0.7%). Most zero-area observations occur 1995-1999 (78.7%; Figure 3) and are located in northeastern Siberia (50%). Following 1999, zero area lakes are less common, remaining consistently under 2.5% of all lakes in the extended GLCP from 2000 through 2020 (Figure 3). Pekel et al. (2016) likewise documented this issue, where the operation of only one Landsat satellite 1995-1999 contributed to few images being collected in northern Siberia. These zero area observations can be indicative of at least four situations. First, zeros could represent a lake drying up, where zero surface area actually indicates no water. Second, zeros could represent real missing (NA) values from incomplete Landsat coverage for certain

locations and years. Third, zero area values could represent a mis-identified HydroLAKES polygon, where the polygon is either not located over water or the algorithms used to create HydroLAKES falsely classified an area as a lake. Fourth, zero values could be due to permanently frozen lakes when the JRC algorithm does not identify a pixel of ice as "water". The position of a zero within a time series in addition to localized insight may aid end users in identifying why a lake was attributed with zero area. For example, a single zero area estimate in the middle of a time series may indicate a lake drying and refilling, whereas a zero value estimated in the years 1995-1999 may indicate poor Landsat coverage. In any case, user prudence will be required for understanding why a lake could be assigned a value of zero and how erroneous zero-area estimates may influence a particular research question or application.

For monthly zero area estimates, the greatest uncertainty of zero-area lakes stems from the quality of Landsat images collected in a given month. In particular, excessive cloud cover can mask water, meaning that exceptionally cloudy times of the year may experience lower chances of observing water. This phenomenon is documented in Pekel et al. (2016), where regions with prolonged seasonal cloudiness experience fewer valid water observations, even as additional Landsat satellites are added into orbit. Consequently, the extended GLCP's monthly lake area estimates are limited by the Landsat imagery from which they are derived. Times and locations lacking valid water pixels result in non-value area estimates (i.e., NA), whereas zero-area estimates represent times when a lake was estimated as having zero surface area. As with annual surface area metrics, understanding why a lake has a monthly area of zero will require user prudence, especially as these estimates may stem from complex local hydrological, climatological, or remote sensing peculiarities.

Assessment of Intra-annual and Interannual Variability

To ensure that variables with known phenologies retained those patterns during data harmonization, we visually assessed if cross-seasonal patterns reflected anticipated phenologies. For climate variables, we confirmed that temperature, precipitation, specific humidity, and shortwave radiation were highest in the summer months and lower in winter months, for both the Northern and Southern Hemispheres (Figure 4; Supplementary figures S1-6). In contrast, longwave radiation values were lowest during June, July, and August in both the Northern and Southern Hemispheres, as expected (Figure 4). For ice and snow data, we confirmed that maximum snow and ice extents in the Northern Hemisphere occurred during December, January, and February, whereas maximum extents in the Southern Hemisphere occurred during June, July, and August (Figure 4; Supplementary figures S7-8). Conversely, we confirmed that minimum values for ice and snow extent occurred during June, July, and August in the Northern Hemisphere and during December, January, and February in the Southern Hemisphere (Figure 4; Supplementary figures 7-8).

As lake area extents do not have uniform broad-scale phenologies, we compared monthly water surface area estimates against HydroLAKES static areas. To assess how frequently and when lake area estimates deviated from HydroLAKES defined areas, we assessed the distribution of the ratio of JRC-derived lake area to the area reported in HydroLAKES. We anticipated that times of the year with greater cloud cover, especially in northern boreal regions, would lead to greater deviations in lake area during winter months. As expected, the difference between

monthly JRC-derived estimates and HydroLAKES-derived estimates varied considerably over a year. Monthly lake area estimates from June through August were more similar to their HydroLAKES areas (Figure 5), although zero-area estimates at the monthly timestep are still pervasive in the dataset. These patterns likely stem from most lakes being concentrated in the Northern Hemisphere, and observations made in non-summer months tend to have greater interference from clouds and ice, thereby resulting in NA values for monthly surface area. Nevertheless, the general congruence between JRC-derived monthly areas during June, July, and August and HydroLAKES static areas gives confidence in the quality of sub-annual area measurements.

For annual lake surface areas, we plotted how the sum of seasonal and permanent areas in a given year compared with static HydroLAKES areas (Figure 6). As with monthly lake area, we assessed the distribution of the ratio of JRC-derived lake area to the area reported in HydroLAKES. We anticipated that years with less satellite cover at northern latitudes would produce greater zero-area estimates, which should disappear in the time series. As expected, data from 1995 through 1999 contained a greater number of zero-area lakes, which decreased after 2000. These deviations likely stem from limited coverage of land surfaces as expanded upon in Pekel et al. (2016). As discussed in Meyer et al. (2020), these deviations are expected and without ground-truthed observations, so there may be no feasible way to gap-fill these data before 1999. Even with these zero-area lakes, most annual estimates were concentrated around the value of the HydroLAKES-reported area.

Manual Quality Control

As with the previous version of the GLCP, we performed intensive analyses on a spatially stratified subset of the data. Lakes were subsampled using the same stratified random subsample described in Meyer et al. (2020). These lakes were meant to capture a global distribution of lakes across all continents. Using this subset, we calculated percent differences, defined as $\frac{x_t - x_{t+1}}{\frac{x_t + x_{t+1}}{2}} * 100$, for all year-month lake combinations and then assessed the magnitude to which percent differences diverged from zero. Percent difference values can range from -200% to 200%, indicating a value going from zero to non-zero or vice-versa for two consecutive time points. For example, a lake having an area of zero in one year and non-zero in the next would have a percent difference of 200%. As expected, all values exhibited small changes inter-annually (Figure 7), indicating that data integrity did not degrade during the harmonization process.

Comparison to Existing Datasets

To date, the GLCP is the only data product that harmonizes climate, human population, and lake area data into a tabular, analysis-ready format. However, there are several datasets that address individual variables contained within the GLCP. Each of these datasets may implement alternative harmonization procedures, and therefore, they should not be considered as identical or immediately substitutable values for existing GLCP variables. For example, ReaLSAT is a global compendium of lake and reservoir surface area that uses HydroLAKES and the JRC to create a time series of waterbody surface areas (Khandelwal et al. 2022). Whereas ReaLSAT uses water occurrence as a filter to remove potentially spurious water pixels, the GLCP evaluates

the ratio of lake expansion for a series of buffers for an individual lake, and then applies a 90-m buffer to all shapefiles. Given these differences, water area estimates between ReaLSAT and the GLCP are derived from identical parent datasets, yet lake area estimates may vary between these products. End users interested in identifying trends in monthly lake surface area through time or investigating shifts in lake area phenology may need to confirm whether trends identified in one dataset are upheld in the other, depending on the nature of the specific research question at hand.

Beyond the climate variables already included in the GLCP, there are several climate datasets that may be more appropriate for specific research questions. The GLCP natively ingests the MERRA-2 dataset. Users looking to compare a particular climate reanalysis dataset with the MERRA-2 derived data can refer to Meyer et al. (2020) for a schematic of how comparisons were made between the GLCP and other climate reanalysis datasets.

Data Use and Recommendations for Reuse

Building upon the previous version of the GLCP (Meyer et al. 2020), the extended GLCP provides an initial foundation for sub-annual, global scale synthesis of lakes' contribution to the hydrologic cycle. The addition of lake ice extent, snow basin cover, and basin-wide humidity expand the degree to which the hydrologic cycle is represented in the GLCP. The use of HydroLAKES to identify waterbodies within the GLCP allows for compatible hydrologic datasets to fill remaining gaps in hydrologic processes. For example, Zhao et al. (2022) includes monthly estimates of lake-specific, volumetric evaporation, which can be joined to the extended GLCP via each lake's specific lake identifier (i.e., Hylak_id). Considering the growing repository of HydroLAKES-derived data products, the GLCP can be used as a scaffold to which complementary, interoperable datasets can add components of the water cycle, thereby enabling more detailed water balance analyses.

Looking beyond how the GLCP can support research on water quantity, the increasing availability of continental-scale water quality datasets creates additional capacity to examine interconnections of water quantity and quality. LimnoSat-US (Topp et al. 2020), AquaSat (Ross et al. 2019), the GLObal Reflectance community dataset for Imaging and optical sensing of Aquatic environments (GLORIA; Lehmann et al. 2023), the national-scale modeled skin temperature dataset (Willard et al. 2021), and the Lake Trophic State - US (LTS-US; Meyer et al. 2024b) are among the most spatially and temporally extensive datasets that enable tracking changes in freshwater ecosystem integrity. Ranging from analysis-ready data for model building (i.e., AquaSat and GLORIA) to derived lake properties (i.e., LimnoSat-US and LTS-US), these datasets present immense potential for tracking changes in lake water quality, which can then be contextualized with co-located shifts in water quantity (Ellis et al. 2024). Furthermore, advances in remote sensing technologies and machine learning methodologies can bolster our understanding of ecosystems less well represented in the aquatic sciences literature, such as tropical (Virdis et al. 2024) and high elevation (Oleksy et al. 2022) lakes. With a monthly estimate of lake surface extent, coupled monthly climate variables, and information on lake ice and surrounding snow extent, the extended GLCP is a powerful tool capable of addressing key aquatic science questions and contextualizing lake ecosystem change across spatial and temporal scales.

Acknowledgements

We would like to thank the following individuals for diverse technical and creative support: The Washington State University Center for Institutional Research Computing, Rohit Dhariwal, and Jennifer C. Adam for computing advice and expertise; Joshua A. Culpepper, Aman Basu, Kirill S. Shchapov for reviewing the dataset for integrity and ease of use; Stephanie G. Labou and Matthew R.V. Ross for reviewing a previous version of this manuscript. This work was funded in part by an NSF GRF (DGE-1347973), a Mendenhall Fellowship from the USGS Water Resources Mission Area, and the USGS Saline Lakes Project. Any use of trade, firm, or product names is for descriptive purposes only and does not imply endorsement by the U.S. Government.

References

Carr, D., ported by N. Lewin-Koh, M. Maechler, and contains copies of lattice functions written by D. Sarkar. 2021. hexbin: Hexagonal Binning Routines.

Dowle, M., and A. Srinivasan. 2021. data.table: Extension of `data.frame`.

Doxsey-Whitfield, E., K. MacManus, S. B. Adamo, L. Pistolesi, J. Squires, O. Borkovska, and S. R. Baptista. 2015. Taking Advantage of the Improved Availability of Census Data: A First Look at the Gridded Population of the World, Version 4. Papers in Applied Geography **1**: 226–234. doi:10.1080/23754931.2015.1014272

Ellis, E. A., G. H. Allen, R. M. Riggs, H. Gao, Y. Li, and C. C. Carey. 2024. Bridging the divide between inland water quantity and quality with satellite remote sensing: An interdisciplinary review. WIREs Water **n/a**: e1725. doi:10.1002/wat2.1725

Gelaro, R., W. McCarty, M. J. Suárez, and others. 2017. The Modern-Era Retrospective Analysis for Research and Applications, Version 2 (MERRA-2). J. Climate **30**: 5419–5454. doi:10.1175/JCLI-D-16-0758.1

Gillies, S. and others. 2013. Rasterio: geospatial raster I/O for Python programmers.

Gorelick, N., M. Hancher, M. Dixon, S. Ilyushchenko, D. Thau, and R. Moore. 2017. Google Earth Engine: Planetary-scale geospatial analysis for everyone. Remote Sensing of Environment **202**: 18–27. doi:10.1016/j.rse.2017.06.031

Grolemund, G., and H. Wickham. 2011. Dates and Times Made Easy with lubridate. Journal of Statistical Software **40**: 1–25.

Hall, D. K., and G. A. Riggs. 2011. Normalized-Difference Snow Index (NDSI), p. 779–780. *In* V.P. Singh, P. Singh, and U.K. Haritashya [eds.], Encyclopedia of Snow, Ice and Glaciers. Springer Netherlands.

Hall, D. K., G. A. Riggs, V. V. Salomonson, N. E. DiGirolamo, and K. J. Bayr. 2002. MODIS snow-cover products. Remote Sensing of Environment **83**: 181–194. doi:10.1016/S0034-4257(02)00095-0

Harris, C. R., K. J. Millman, S. J. van der Walt, and others. 2020. Array programming with NumPy. Nature **585**: 357–362. doi:10.1038/s41586-020-2649-2

Hersbach, H., B. Bell, P. Berrisford, and others. 2020. The ERA5 global reanalysis. Quarterly Journal of the Royal Meteorological Society **146**: 1999–2049. doi:10.1002/qj.3803

Iannone, R. 2022. DiagrammeR: Graph/Network Visualization.

Jones, I. D., and J. P. Smol, eds. 2023. Wetzel's Limnology: Lake and River Ecosystems, 4th edition. Academic Press.

Jones, J. W. 2019. Improved Automated Detection of Subpixel-Scale Inundation—Revised Dynamic Surface Water Extent (DSWE) Partial Surface Water Tests. Remote Sensing **11**: 374. doi:10.3390/rs11040374

Jordahl, K. 2014. GeoPandas: Python tools for geographic data. URL: https://github.com/geopandas/geopandas.

Khandelwal, A., A. Karpatne, P. Ravirathinam, R. Ghosh, Z. Wei, H. A. Dugan, P. C. Hanson, and V. Kumar. 2022. ReaLSAT, a global dataset of reservoir and lake surface area variations. Sci Data **9**: 356. doi:10.1038/s41597-022-01449-5

Labou, S. G., M. F. Meyer, M. R. Brousil, A. N. Cramer, and B. T. Luff. 2019. Global lake area, climate, and population dataset.

Lehmann, M. K., D. Gurlin, N. Pahlevan, and others. 2023. GLORIA - A globally representative hyperspectral in situ dataset for optical sensing of water quality. Sci Data **10**: 100. doi:10.1038/s41597-023-01973-y

Lehner, B., and G. Grill. 2013. Global river hydrography and network routing: baseline data and new approaches to study the world's large river systems. Hydrological Processes **27**: 2171–2186. doi:10.1002/hyp.9740

McKinney, W. and others. 2010. Data structures for statistical computing in python. *Proceedings of the 9th Python in Science Conference*. Austin, TX. 51–56.

Messager, M. L., B. Lehner, G. Grill, I. Nedeva, and O. Schmitt. 2016. Estimating the volume and age of water stored in global lakes using a geo-statistical approach. Nature Communications **7**: 1–11. doi:10.1038/ncomms13603

Met Office. 2010. Cartopy: a cartographic python library with a Matplotlib interface.

Meyer, M. F., M. R. Brousil, S. G. Virdis, and others. 2024a. The Extended Global Lake area, Climate, and Population Dataset (GLCP). Environmental Data Initiative. doi.org/10.6073/pasta/e0bf4571ca6cbfb81c3ed7caefc85fc6

Meyer, M. F., S. G. Labou, A. N. Cramer, M. R. Brousil, and B. T. Luff. 2020. The global lake area, climate, and population dataset. Sci Data **7**: 174. doi:10.1038/s41597-020-0517-4

Meyer, M. F., S. N. Topp, T. V. King, and others. 2024b. National-scale remotely sensed lake trophic state from 1984 through 2020. Sci Data **11**: 77. doi:10.1038/s41597-024-02921-0

Oleksy, I. A., S. M. Collins, S. J. Sillen, and others. 2022. Heterogenous controls on lake color and trends across the high-elevation U.S. Rocky Mountain region. Environ. Res. Lett. **17**: 104041. doi:10.1088/1748-9326/ac939c

O'Reilly, C. M., S. Sharma, D. K. Gray, and others. 2015. Rapid and highly variable warming of lake surface waters around the globe. Geophysical Research Letters **42**: 10,773-10,781. doi:10.1002/2015GL066235

Pekel, J.-F., A. Cottam, N. Gorelick, and A. S. Belward. 2016. High-resolution mapping of global surface water and its long-term changes. Nature **540**: 418–422. doi:10.1038/nature20584

R Core Team. 2022. R: A Language and Environment for Statistical Computing.

Ross, M. R. V., S. N. Topp, A. P. Appling, X. Yang, C. Kuhn, D. Butman, M. Simard, and T. M. Pavelsky. 2019. AquaSat: A Data Set to Enable Remote Sensing of Water Quality for Inland Waters. Water Resources Research **55**: 10012–10025. doi:10.1029/2019WR024883

Topp, S. N., T. M. Pavelsky, H. A. Dugan, X. Yang, J. R. Gardner, and M. R. V. Ross. 2020. Shifting patterns of lake color phenology in over 26,000 US lakes. Earth and Space Science Open Archive. doi:10.1002/essoar.10504667.1

Verdin, K. L., and J. P. Verdin. 1999. A topological system for delineation and codification of the Earth's river basins. Journal of Hydrology **218**: 1–12. doi:10.1016/S0022-1694(99)00011-6

Verpoorter, C., T. Kutser, D. A. Seekell, and L. J. Tranvik. 2014. A global inventory of lakes based on high-resolution satellite imagery. Geophysical Research Letters **41**: 6396–6402. doi:10.1002/2014GL060641

Virdis, S. G. P., S. Kongwarakom, L. Juneng, B. M. Padedda, and S. Shrestha. 2024. Historical and projected response of Southeast Asian lakes surface water temperature to warming climate. Environmental Research **247**: 118412. doi:10.1016/j.envres.2024.118412

Vörösmarty, C. J., P. Green, J. Salisbury, and R. B. Lammers. 2000. Global water resources: vulnerability from climate change and population growth. science **289**: 284–288.
Vörösmarty, C. J., V. Rodríguez Osuna, A. D. Cak, and others. 2018. Ecosystem-based water security and the Sustainable Development Goals (SDGs). Ecohydrology & Hydrobiology **18**: 317–333. doi:10.1016/j.ecohyd.2018.07.004
Webb, E. E., A. K. Liljedahl, J. A. Cordeiro, M. M. Loranty, C. Witharana, and J. W. Lichstein. 2022. Permafrost thaw drives surface water decline across lake-rich regions of the Arctic. Nat. Clim. Chang. **12**: 841–846. doi:10.1038/s41558-022-01455-w
Wickham, H. 2019. stringr: Simple, Consistent Wrappers for Common String Operations.
Wickham, H., M. Averick, J. Bryan, and others. 2019. Welcome to the tidyverse. Journal of Open Source Software **4**: 1686. doi:10.21105/joss.01686
Willard, J. D., J. S. Read, A. P. Appling, S. K. Oliver, X. Jia, and V. Kumar. 2021. Predicting Water Temperature Dynamics of Unmonitored Lakes With Meta-Transfer Learning. Water Resources Research **57**: e2021WR029579. doi:10.1029/2021WR029579
Woolway, R. I., B. M. Kraemer, J. D. Lenters, C. J. Merchant, C. M. O'Reilly, and S. Sharma. 2020. Global lake responses to climate change. Nat Rev Earth Environ **1**: 388–403. doi:10.1038/s43017-020-0067-5
Yao, F., B. Livneh, B. Rajagopalan, J. Wang, J.-F. Crétaux, Y. Wada, and M. Berge-Nguyen. 2023. Satellites reveal widespread decline in global lake water storage. Science **380**: 743–749. doi:10.1126/science.abo2812
Zhao, G., Y. Li, L. Zhou, and H. Gao. 2022. Evaporative water loss of 1.42 million global lakes. Nat Commun **13**: 3686. doi:10.1038/s41467-022-31125-6
Zhou, G., W. Liu, C. Xie, and others. 2024. Accelerating thermokarst lake changes on the Qinghai–Tibetan Plateau. Sci Rep **14**: 2985. doi:10.1038/s41598-024-52558-7

Figures and Tables

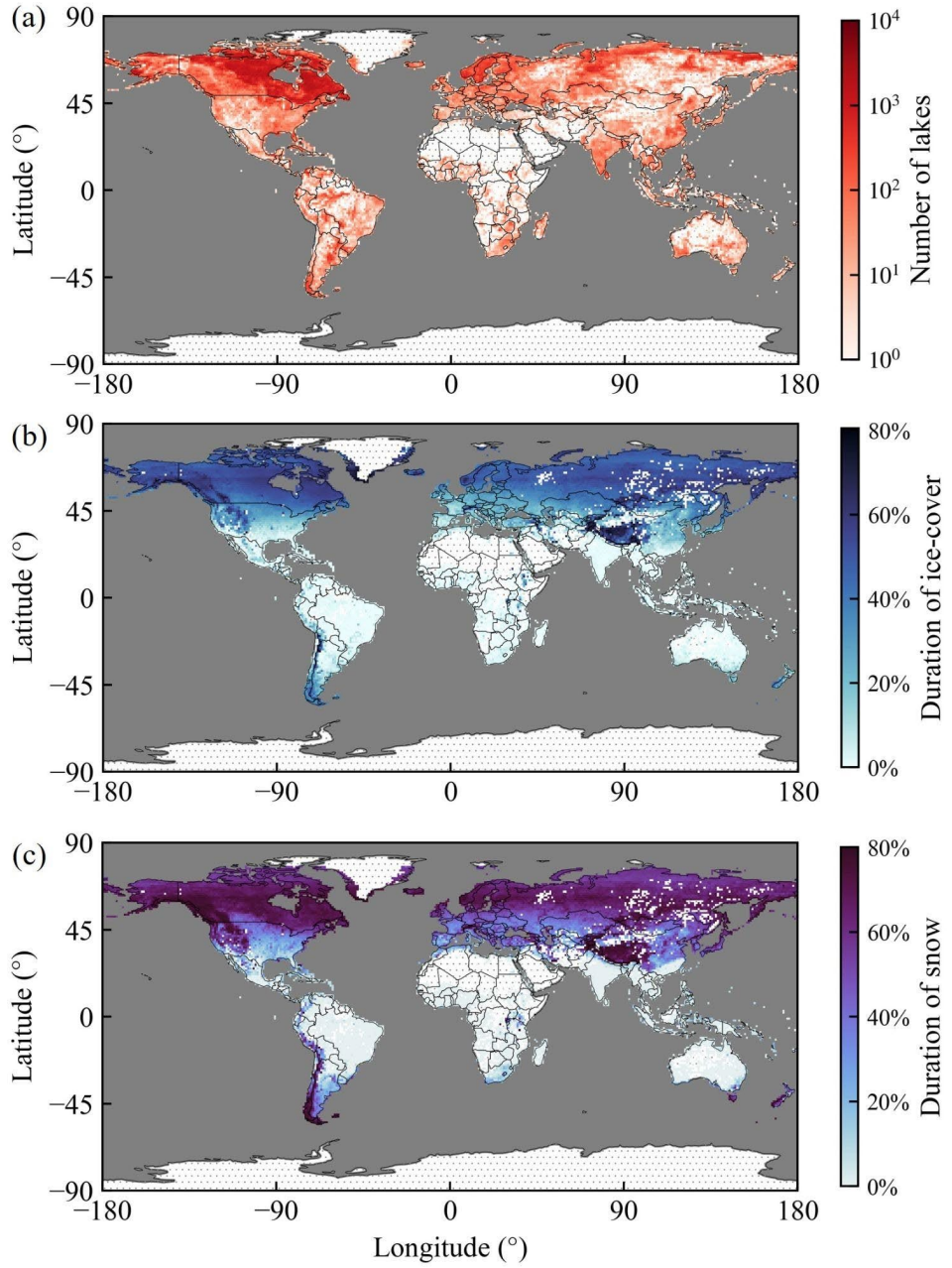

Figure 1: (a) Number of lakes in each 1°×1° cell included in the extended GLCP dataset (Meyer et al. 2024). (b-c) Durations of ice-cover and snow. Duration of ice-cover (or snow) is defined as the ratio of iced (or snowing) months (i.e., mean value > 0) to total months in the period of 1995 to 2020. Data in (b-c) are averaged over lakes for each 1°×1° cell. Hatched areas represent regions included in extended GLCP dataset but where lakes of at least 10 ha do not exist. Maps are made with the cartopy package (Met Office 2010).

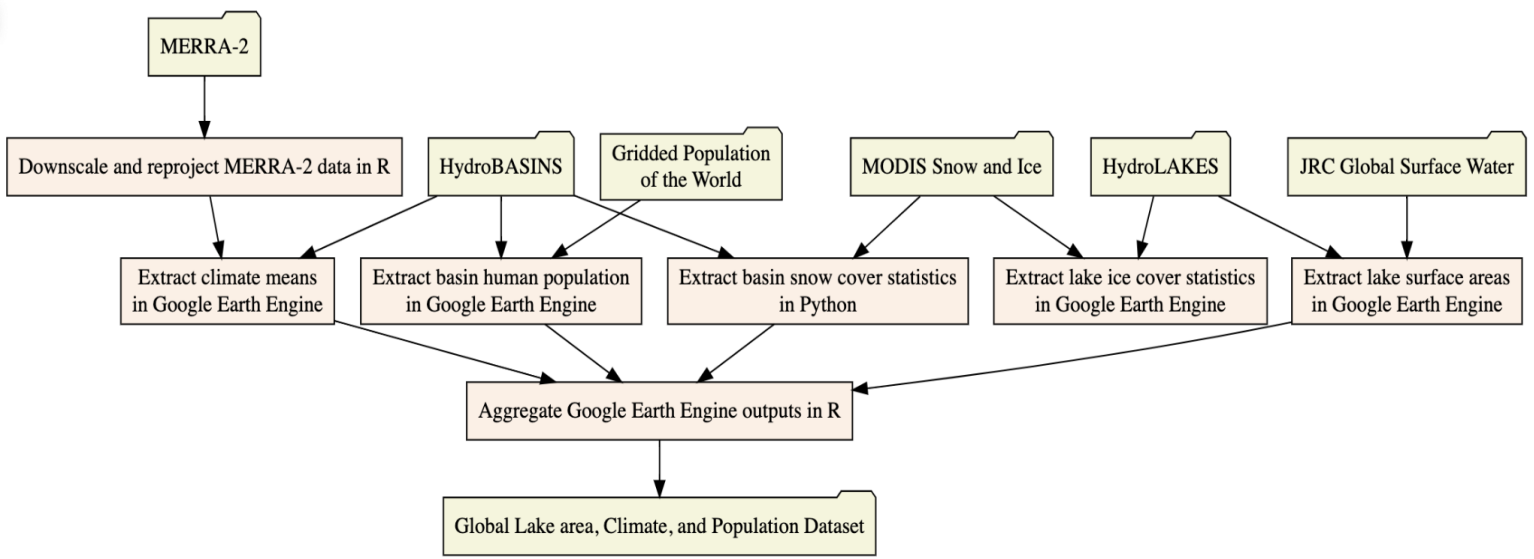

Figure 2: Workflow for compiling the extended Global Lake area, Climate, and Population (GLCP) dataset. File folders represent datasets, whereas rectangles represent processing steps. This flowchart was made using the DiagrammeR package (Iannone 2022).

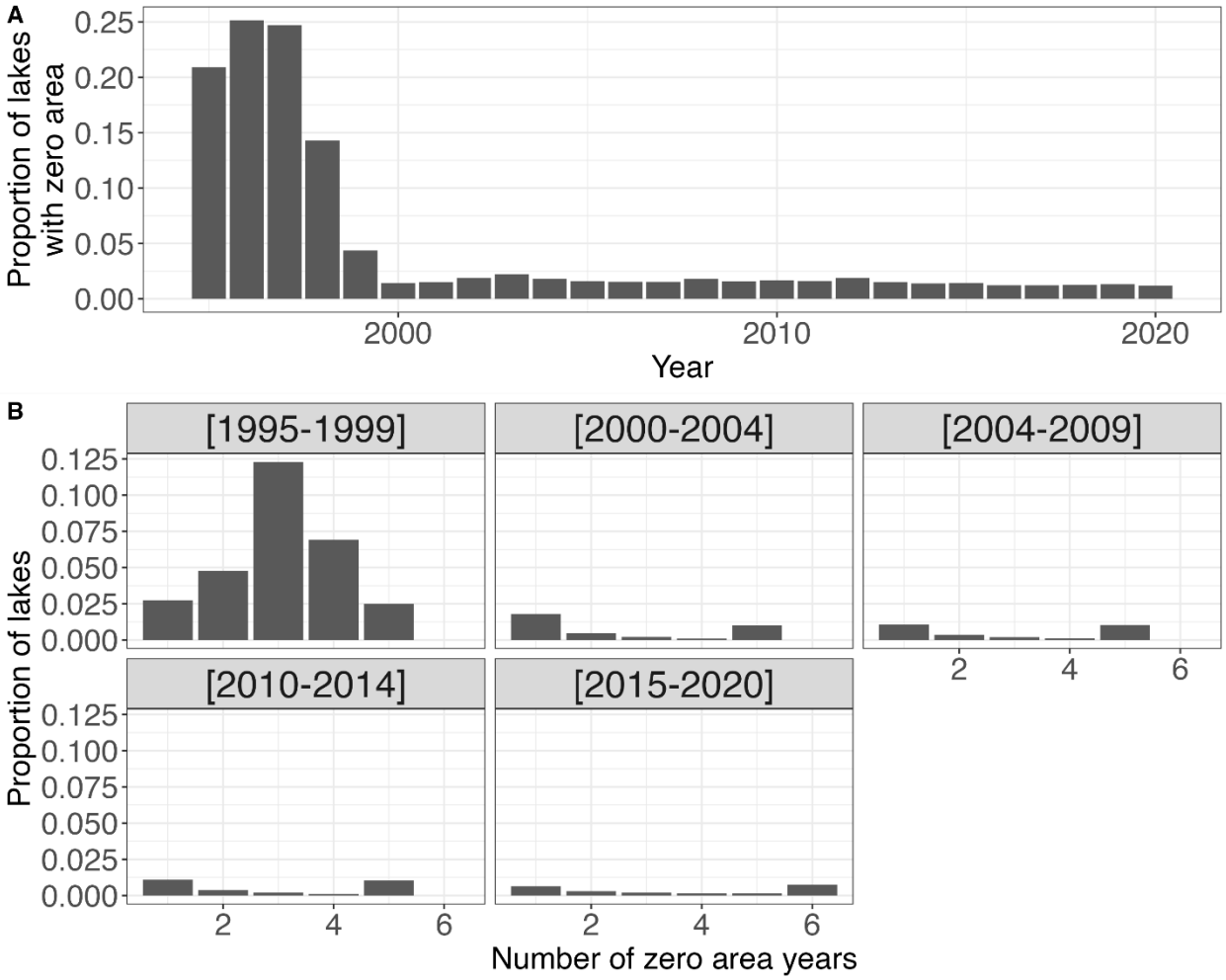

Figure 3: Proportion of lakes in a given year with zero area (A) and frequency of zero-area observations for individual lakes (B) in the extended GLCP dataset (Meyer et al. 2024). To get a sense of when zero area estimates occur, we examined the overall frequency of zero area estimates for all lakes and years. Further, we examined how individual lakes experienced multiple zero area estimates in discrete 5-year epochs. Prior to 2000, zero area estimates tend to be more prevalent in the time series, where most lakes are missing three years of data 1995-1999.

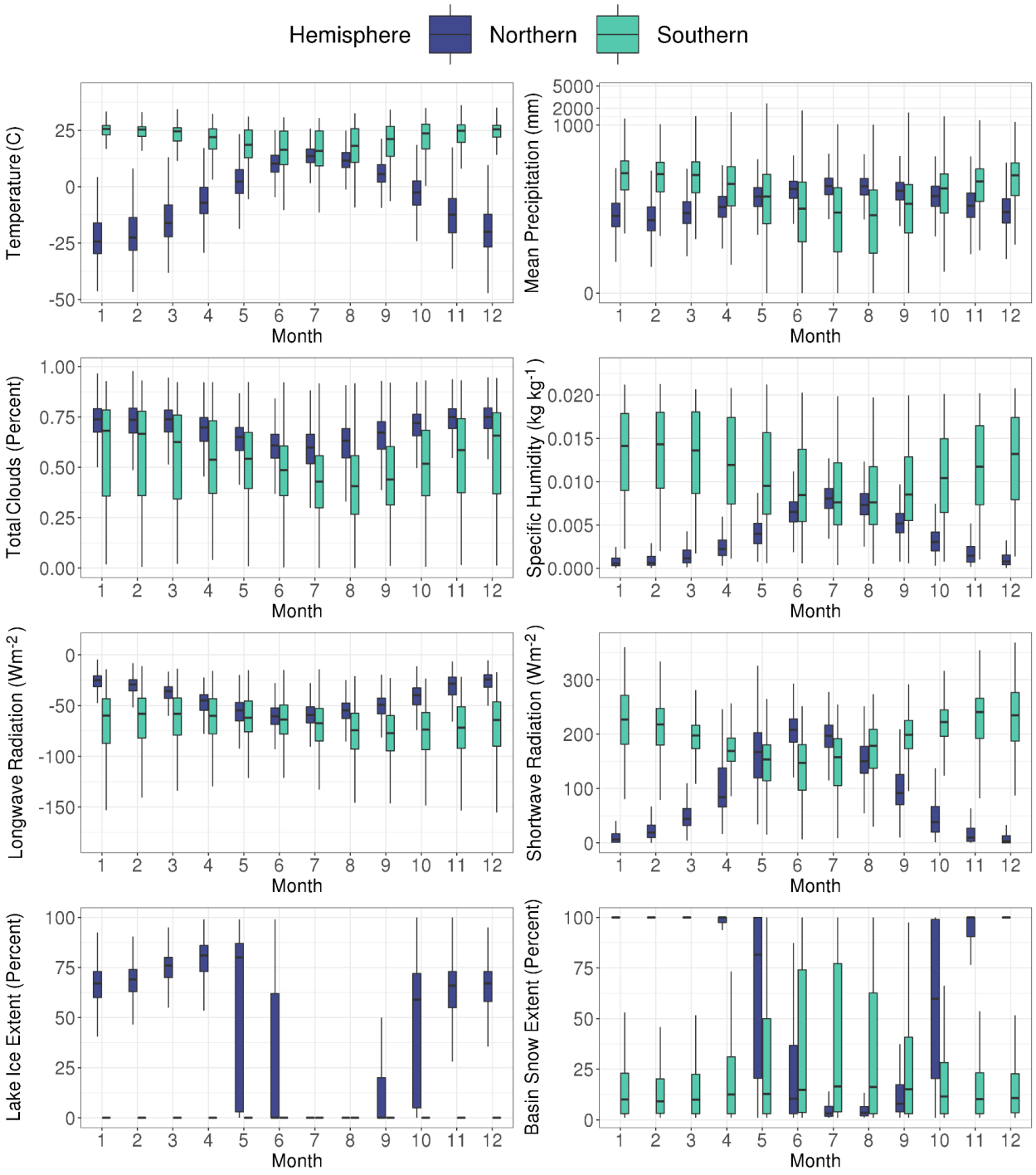

Figure 4: Boxplots of climate variables, lake ice extent, and snow cover in the extended GLCP dataset across all months 1995-2020 in both the Northern and Southern Hemispheres. For readability, outliers, defined as a value exceeding 1.5 times the interquartile range, have been removed from the boxplots, but a version with outliers is included in the supplemental figures (Supplementary figure S9).

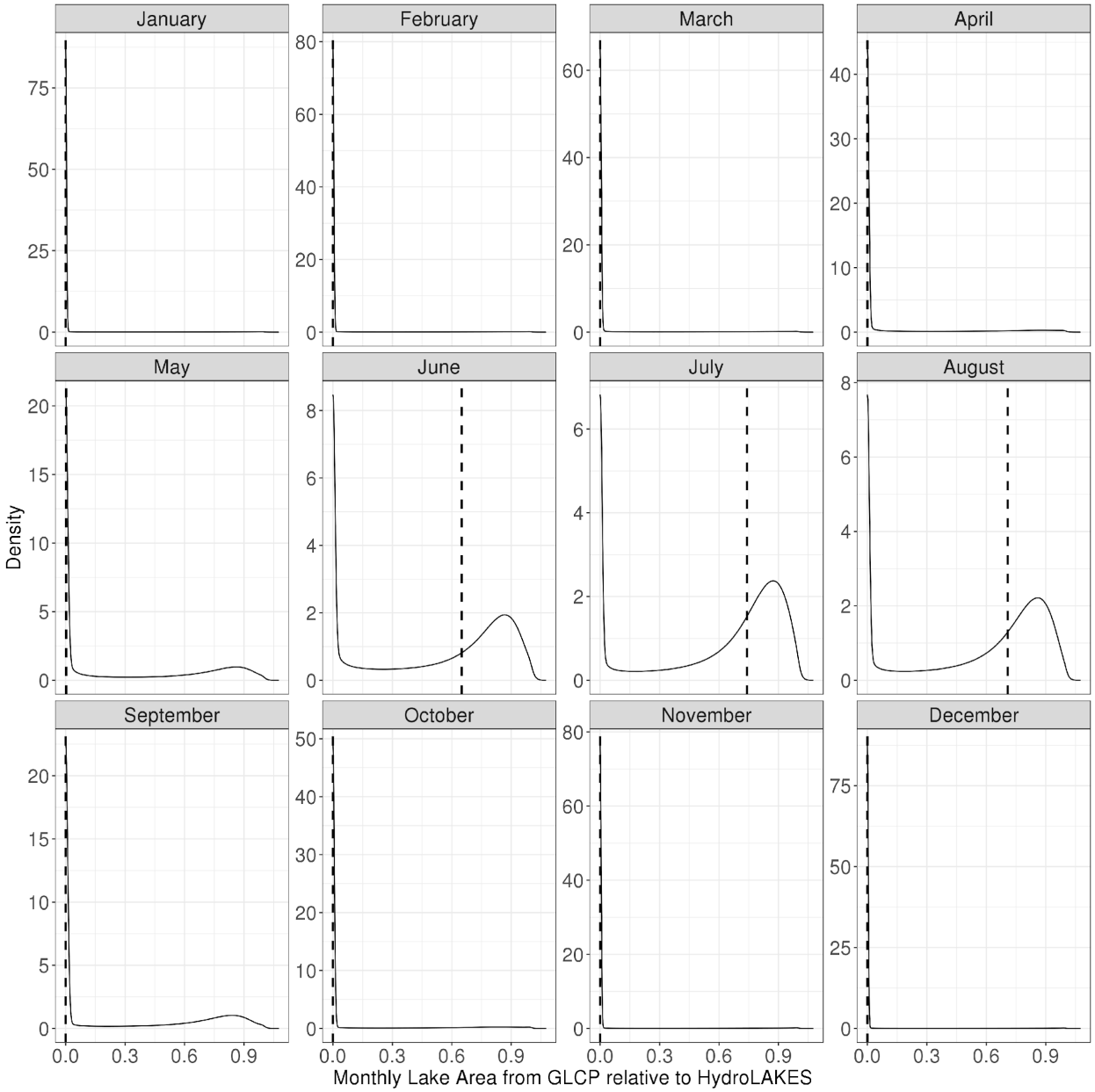

Figure 5: Monthly lake area estimates contained in the extended GLCP dataset (Meyer et al. 2024) compared to static area estimates listed in HydroLAKES (Messager et al. 2016). Values closer to 0 represent lake areas that are smaller than the HydroLAKES reported area. Values closer to 1 represent a closer match between HydroLAKES and Joint Research Centre (JRC) estimated lake areas. The vertical dashed line in each facet represents the mean value in a given month 1995-2020.

Figure 6: Annual lake area estimates contained in the extended GLCP (Meyer et al. 2024) compared to static area estimates listed in HydroLAKES (Meyer et al. 2016). Values closer to 0 represent lake areas that are smaller than the HydroLAKES reported area. Values closer to 1 represent a closer match between HydroLAKES and Joint Research Centre (JRC; Pekel et al. 2016) estimated lake areas . Values greater than 1 represent JRC-derived areas that are greater than HydroLAKES reported areas. The vertical dashed line in each facet represents the mean value in a given year.

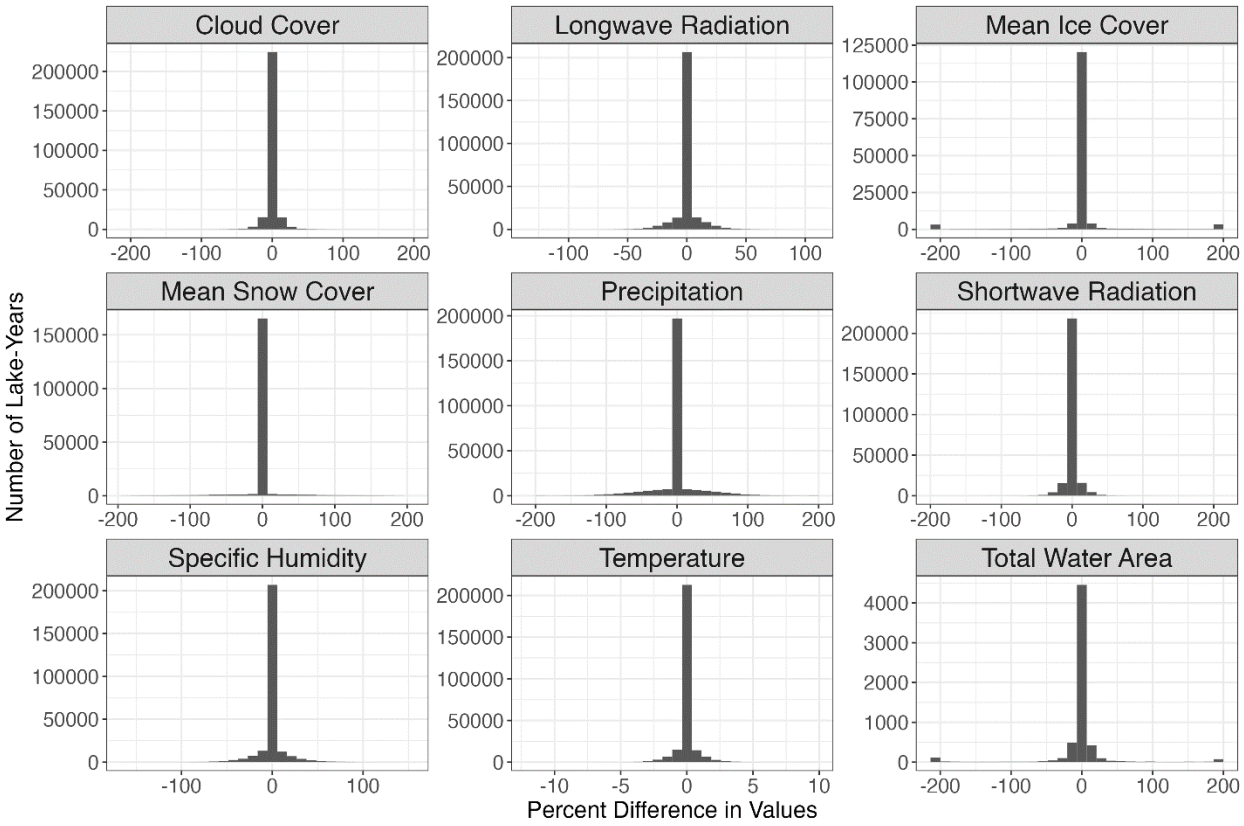

Figure 7: Histograms of percent difference in monthly values for all climate variables, ice extent, snow cover, and annual water area. A value of 200% or -200% represents a timepoint where a lake or basin went from zero to non-zero or non-zero to zero, respectively. Lakes considered in this analysis stem from a spatially stratified random subsample, which was also used in Meyer et al. (2020) for consistency. Qualitatively, all distributions are nearly identical with those observed in Meyer et al. (2020).

Supplemental Figures

Michael F Meyer[1,2], Salvatore GP Virdis[3], Xiao Yang[4], Matthew R Brousil[5], Ryan P McClure[6], Sapna Sharma[7], R Iestyn Woolway[8], Alli N Cramer[9], Jianning Ren[10], Stephen L Katz[11], Stephanie E Hampton[6], Haoran Shi[8]

[1.] U.S. Geological Survey, Water Resources Mission Area, Observing Systems Division - Hydrologic Remote Sensing Branch, Madison, WI, USA
[2.] Center for Limnology, University of Wisconsin - Madison, Madison, WI, USA
[3.] Department of Information & Communication Technologies, School of Engineering and Technology, Asian Institute of Technology, Pathum Thani, Thailand
[4.] Department of Earth Sciences, Southern Methodist University, Dallas, TX, USA
[5.] Ecosystem Science and Sustainability, Colorado State University, Fort Collins, CO, USA
[6.] Biosphere Sciences and Engineering, Carnegie Institution for Science, Pasadena, CA, USA
[7.] Biology Department, York University, Toronto, ON, Canada
[8.] School of Ocean Sciences, Bangor University, Menai Bridge, UK
[9.] School of Mathematical and Natural Sciences, Arizona State University, Phoenix, AZ, USA
[10.] Department of Civil and Environmental Engineering, National University of Singapore, Singapore
[11.] Sharper Informatics Solutions, Seattle, WA, USA

This document contains supplemental figures for the manuscript “The extended Global Lake area, Climate, and Population (GLCP) dataset: Extending the GLCP to include ice, snow, and radiation-related climate variables” by Meyer et al.

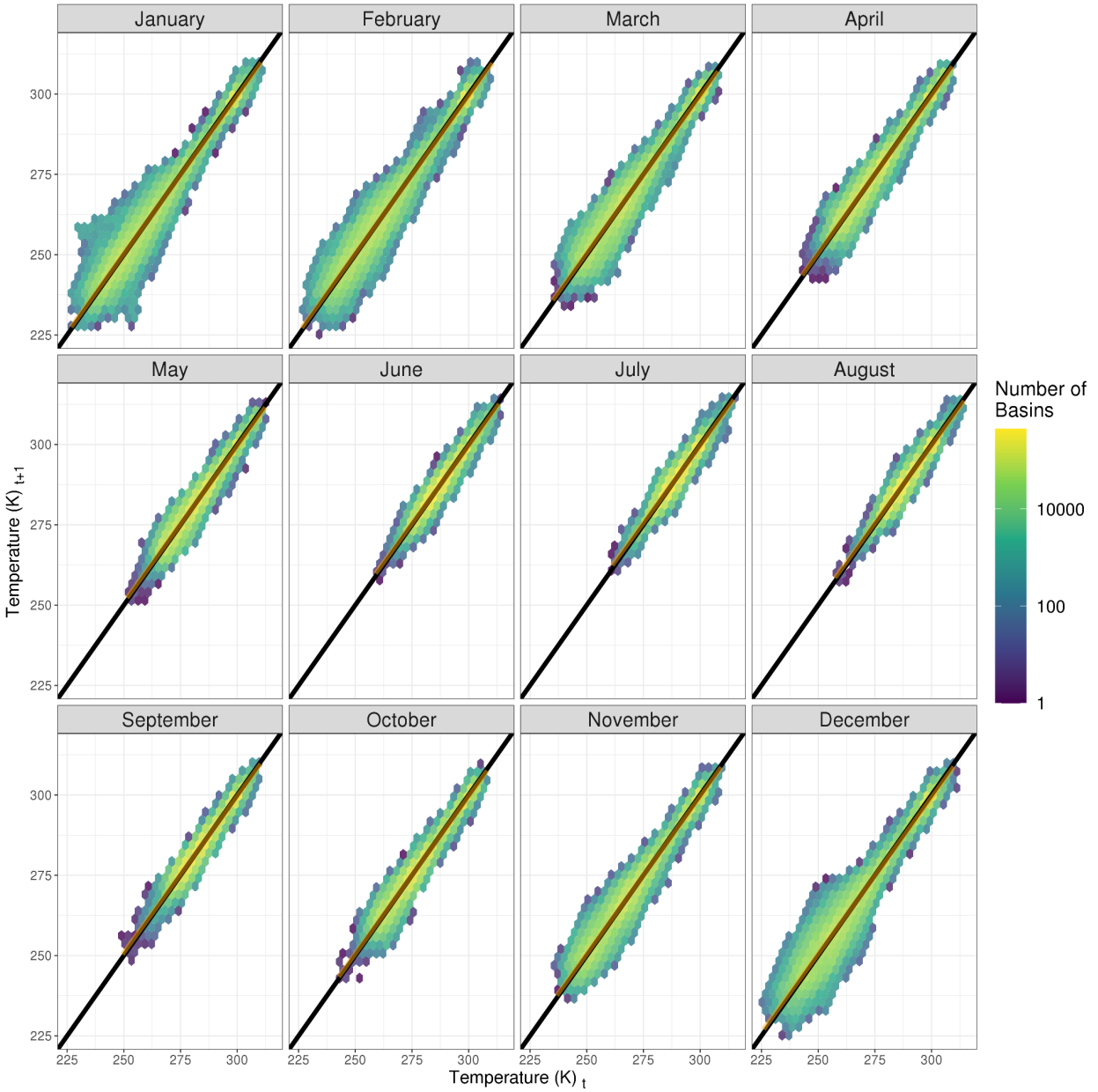

Figure S1: Monthly 1:1 plot for basin 2-m air temperature in the extended GLCP (Meyer et al. 2024). The black line represents the 1:1 line, whereas the transparent orange line represents the linear model fitted to all points. The x-axis represents the temperature of a given year (e.g., 1995), whereas the y-axis represents the temperature in the same basin and month, but in the successive year (e.g., 1996).

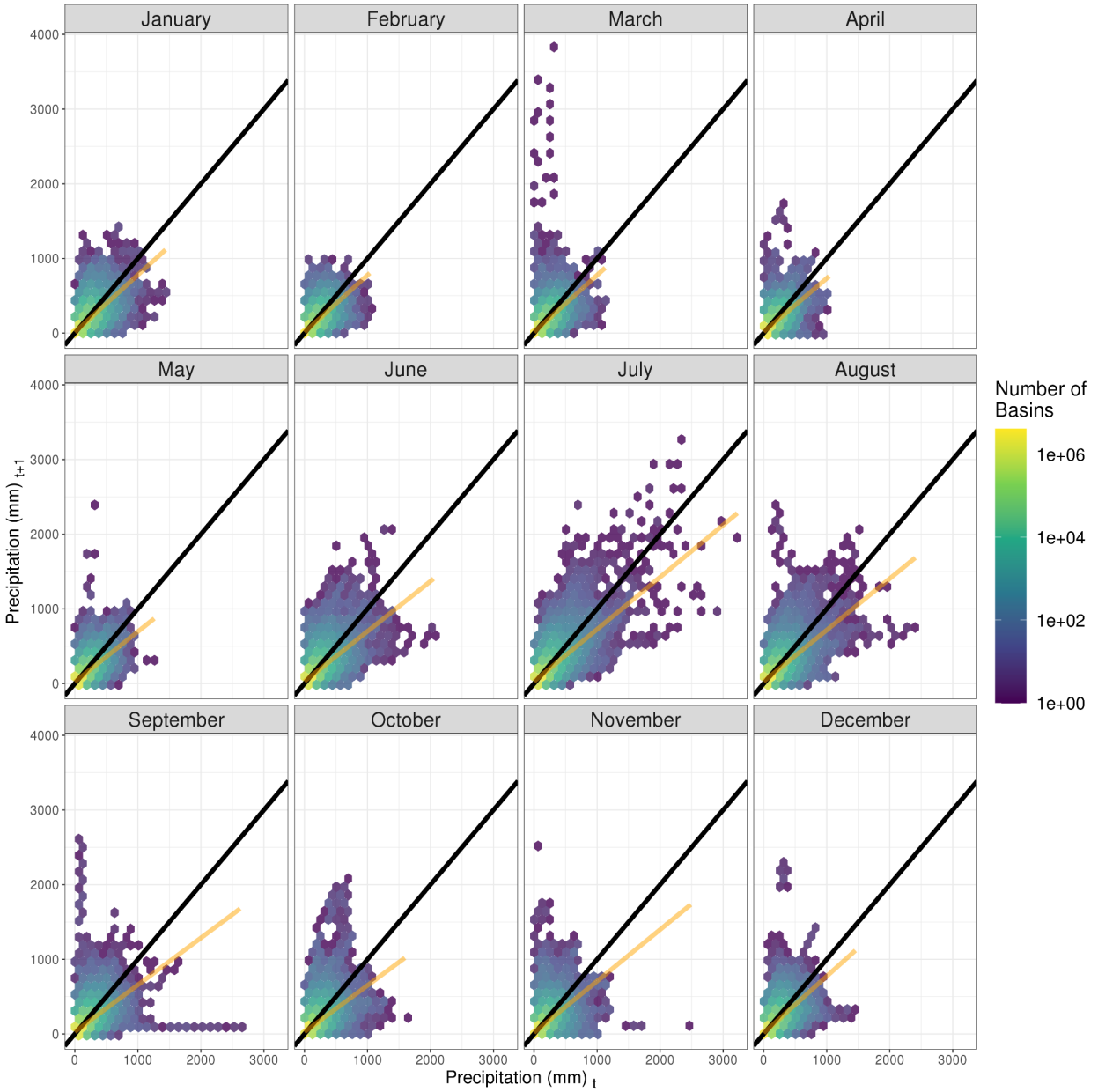

Figure S2: Monthly 1:1 plot for basin precipitation in the extended GLCP (Meyer et al. 2024). The black line represents the 1:1 line, whereas the transparent orange line represents the linear model fitted to all points. The x-axis represents the precipitation of a given year (e.g., 1995), whereas the y-axis represents the precipitation in the same basin and month, but in the successive year (e.g., 1996).

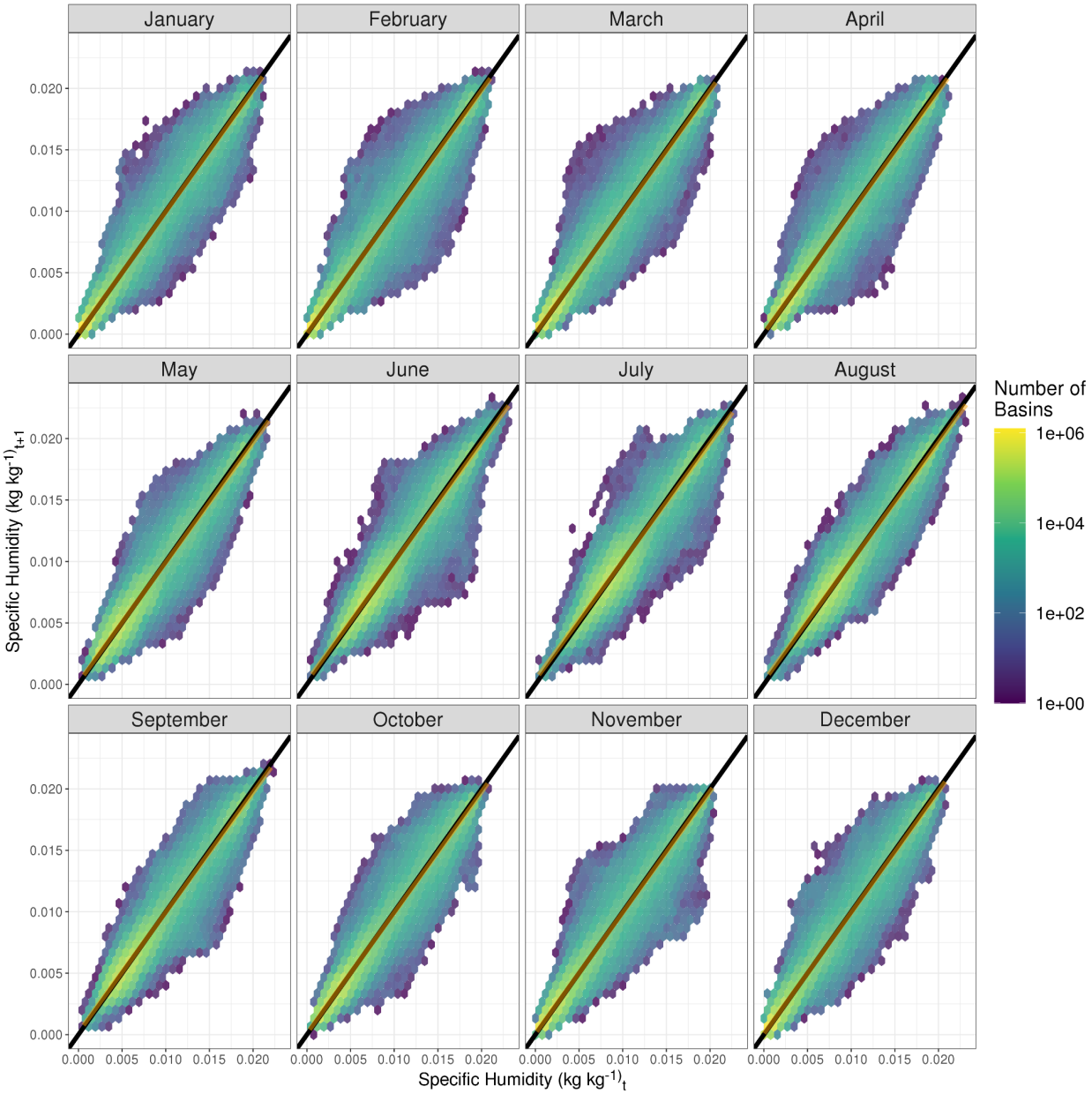

Figure S3: Monthly 1:1 plot for basin 2-m specific humidity in the extended GLCP (Meyer et al. 2024). The black line represents the 1:1 line, whereas the transparent orange line represents the linear model fitted to all points. The x-axis represents the humidity of a given year (e.g., 1995), whereas the y-axis represents the humidity in the same basin and month, but in the successive year (e.g., 1996).

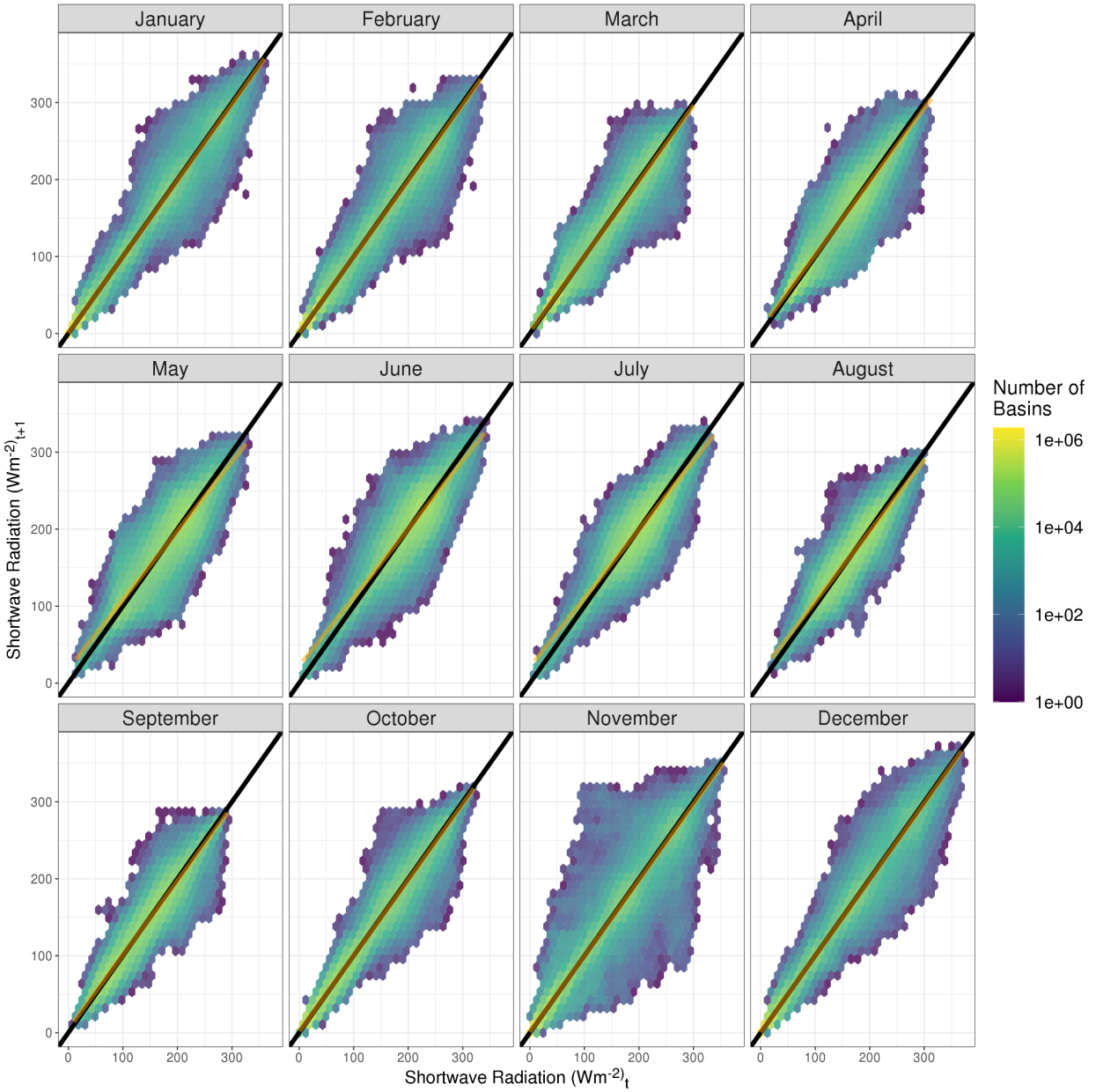

Figure S4: Monthly 1:1 plot for basin net downward shortwave radiation in the extended GLCP (Meyer et al. 2024). The black line represents the 1:1 line, whereas the transparent orange line represents the linear model fitted to all points. The x-axis represents the shortwave radiation of a given year (e.g., 1995), whereas the y-axis represents the shortwave radiation in the same basin and month, but in the successive year (e.g., 1996).

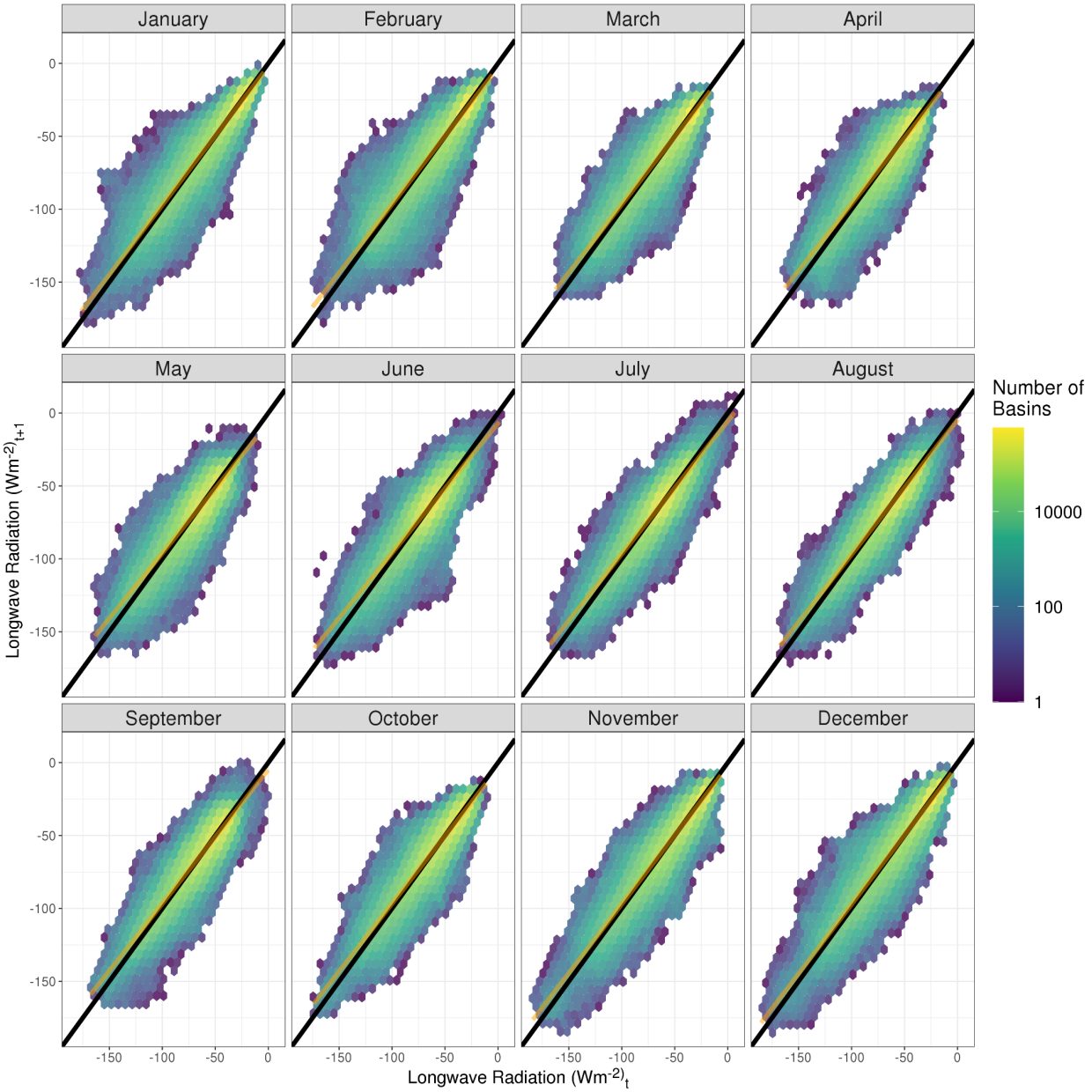

Figure S5: Monthly 1:1 plot for basin net downward longwave radiation in the extended GLCP (Meyer et al. 2024). The black line represents the 1:1 line, whereas the transparent orange line represents the linear model fitted to all points. The x-axis represents the longwave radiation of a given year (e.g., 1995), whereas the y-axis represents the longwave radiation in the same basin and month, but in the successive year (e.g., 1996).

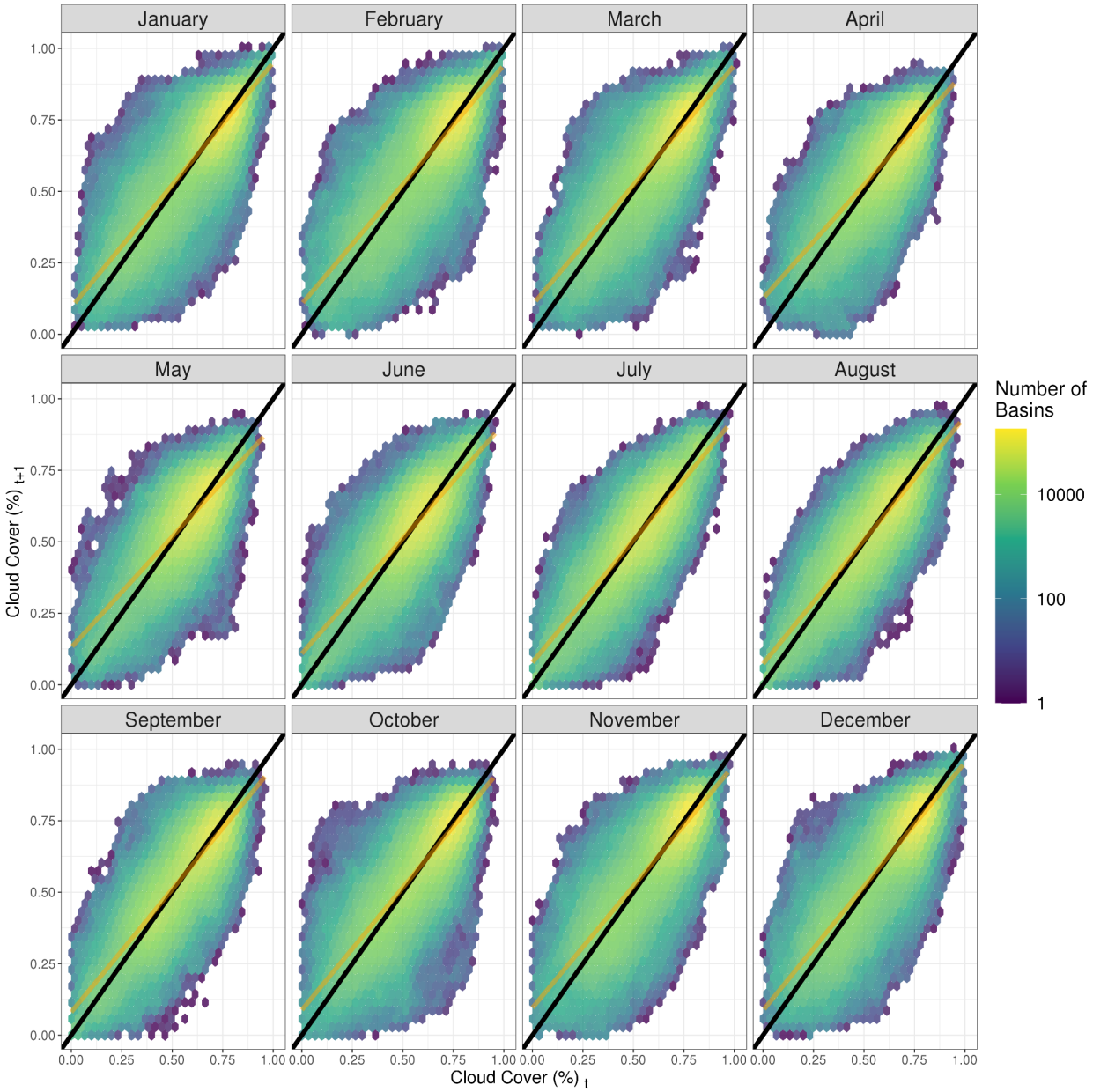

Figure S6: Monthly 1:1 plot for basin fractional cloud cover in the extended GLCP (Meyer et al. 2024). The black line represents the 1:1 line, whereas the transparent orange line represents the linear model fitted to all points. The x-axis represents the fractional cloud cover of a given year (e.g., 1995), whereas the y-axis represents the fractional cloud cover in the same basin and month, but in the successive year (e.g., 1996).

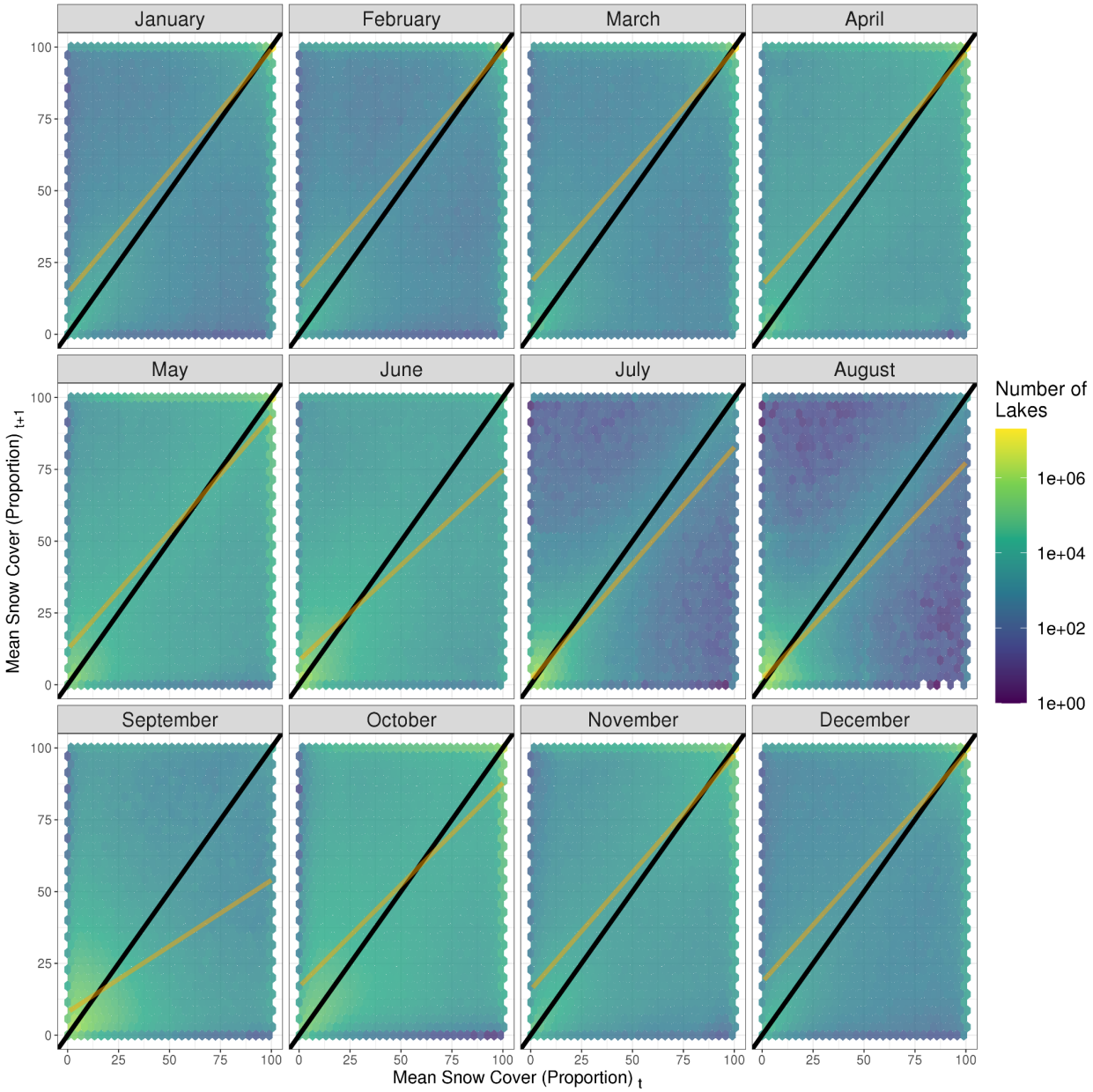

Figure S7: Monthly 1:1 plot for basin mean snow cover in the extended GLCP (Meyer et al. 2024). The black line represents the 1:1 line, whereas the transparent orange line represents the linear model fitted to all points. The x-axis represents the mean snow cover of a given year (e.g., 1995), whereas the y-axis represents the mean snow cover in the same basin and month, but in the successive year (e.g., 1996).

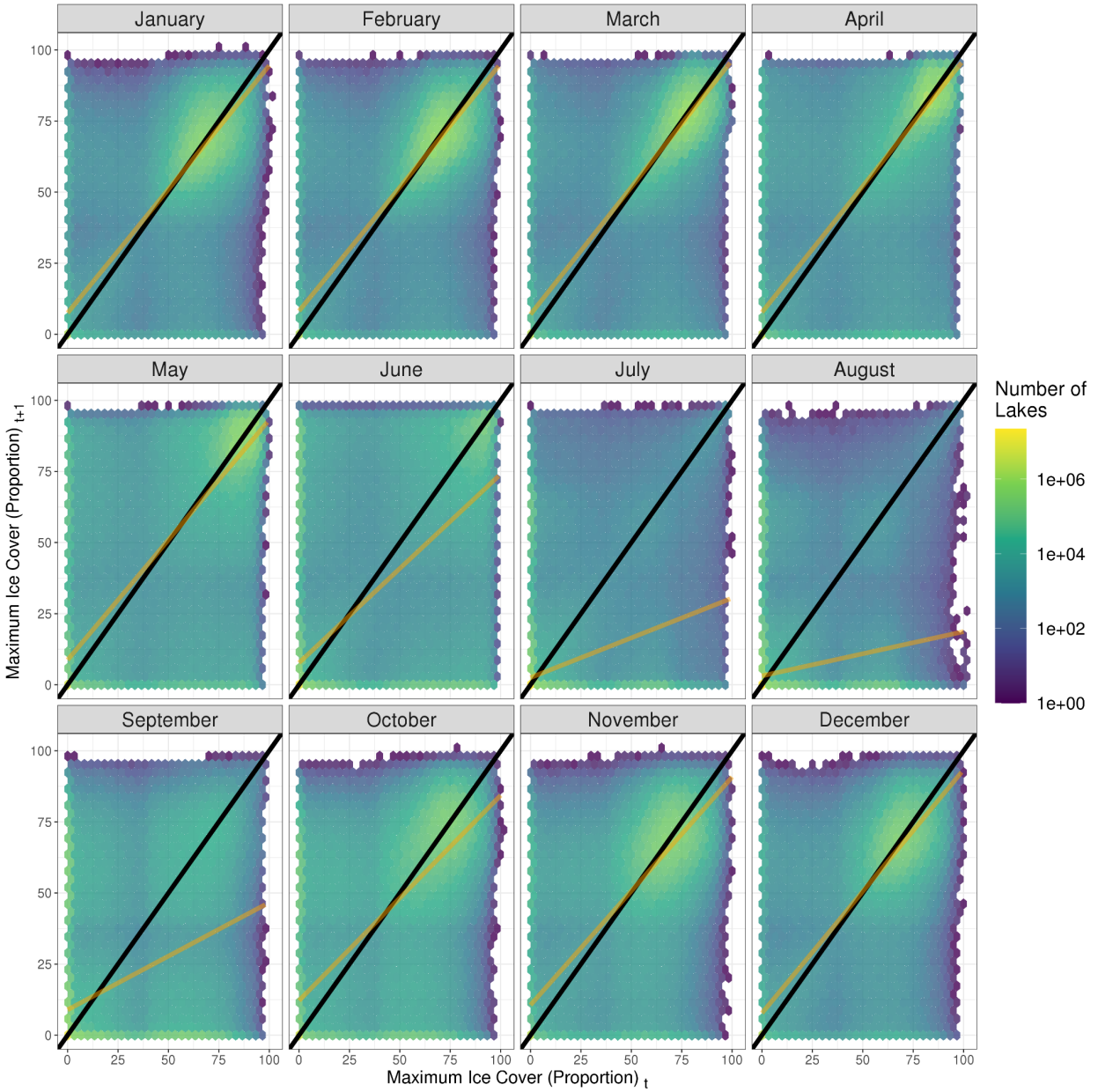

Figure S8: Monthly 1:1 plot for lake maximum ice cover in the extended GLCP (Meyer et al. 2024). The black line represents the 1:1 line, whereas the transparent orange line represents the linear model fitted to all points. The x-axis represents the maximum ice cover of a given year (e.g., 1995), whereas the y-axis represents the maximum ice cover in the same basin and month, but in the successive year (e.g., 1996). Notably, lake ice measurements occur in times that may be less expected. In many cases, this peculiarity is driven by the Moderate Resolution Imaging Spectroradiometer (MODIS) algorithm used to classify lake ice. These occurrences can happen when lakes experience excessively turbid conditions, intense algal blooms, or drying completely. Consequently, we encourage end users to filter ice estimates through temperature, water area measurements, or *in situ* observations to ensure high quality in ice area measurements for their specific question.

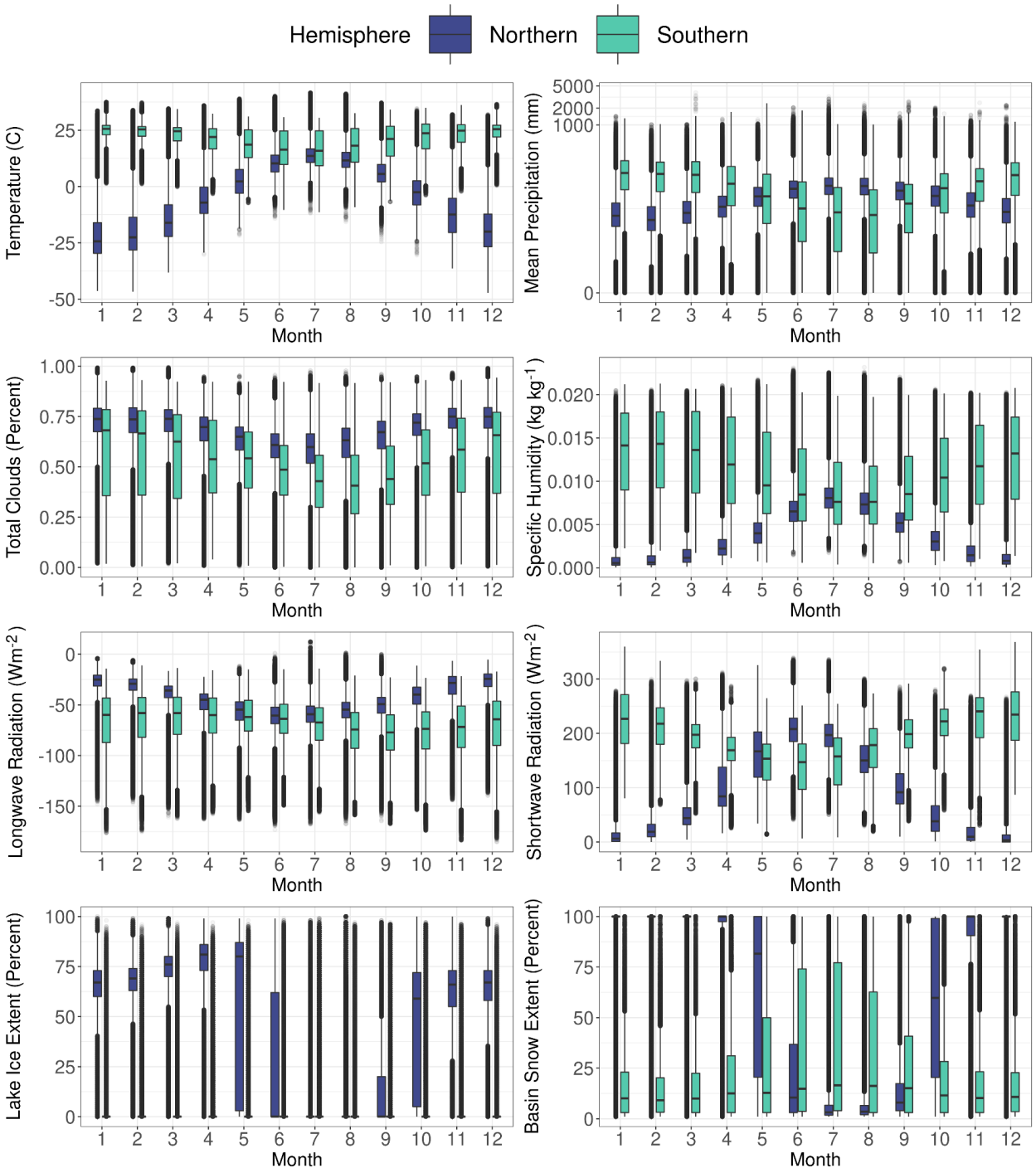

Figure S9: Boxplots of climate variables, lake ice extent, and snow cover in the extended GLCP (Meyer et al. 2024) across all months in both the Northern and Southern Hemispheres.